Wetting, Mixing, and Phase Transitions in Langmuir-Gibbs Films

E. Sloutskin,[1] Z. Sapir,[1] C. D. Bain,[2] Q. Lei,[3] K. M. Wilkinson,[3] L. Tamam,[1] M. Deutsch,[1,*] and B. M. Ocko[4]

[1]*Department of Physics and Institute of Nanotechnology and Advanced Materials, Bar-Ilan University, Ramat-Gan 52900, Israel*
[2]*Department of Chemistry, Durham University, South Road, Durham, DH1 3LE, United Kingdom*
[3]*Department of Chemistry, Oxford University, Mansfield Road, Oxford OX1 3TA, United Kingdom*
[4]*Condensed Matter Physics & Materials Sciences Department, Brookhaven National Laboratory, Upton, New York 11973, USA*

(Received 3 June 2007; published 28 September 2007)

Millimolar bulk concentrations of the surfactant cetyltrimethylammonium bromide (CTAB) induce spreading of alkanes, $H(CH_2)_nH$ (denoted C_n) $12 \leq n \leq 21$, on the water surface, which is not otherwise wet by these alkanes. The novel Langmuir-Gibbs film (LGF) formed is a liquidlike monolayer comprising both alkanes and CTAB tails. Upon cooling, an ordering transition occurs, yielding a hexagonally packed, quasi-2D crystal. For $11 \leq n \leq 17$ this surface-frozen LGF is a crystalline monolayer. For $18 \leq n \leq 21$ the LGF is a bilayer with a crystalline, pure-alkane, upper monolayer, and a liquidlike lower monolayer. The phase diagram and film structure were determined by x-ray, ellipsometry, and surface tension measurements. A thermodynamic theory accounts quantitatively for the observations.

DOI: 10.1103/PhysRevLett.99.136102 PACS numbers: 68.03.Cd, 68.03.Hj, 68.18.Jk

Monolayers of insoluble surfactants have been studied for over a century since the original report by Pockels in 1891 [1]. Commonly known as Langmuir films (LFs), these monolayers have been proposed for a wide range of applications, including nanoelectronics, structural biology, biomimetics, design of optical elements, and water conservation [2]. LFs on water show a rich array of temperature- and surface-pressure-dependent ordered phases [3]. In contrast to LFs, monolayers formed by surface adsorption of soluble surfactants, known as Gibbs films (GFs) [4], rarely exhibit ordered phases [5]. One of the most studied GFs is the cationic surfactant cetyltrimethylammonium bromide (CTAB) $[H(CH_2)_{16}N^+(CH_3)_3Br^-]$. This molecule has a C_{16} alkyl tail, a bulky, positively charged trimethylammonium headgroup (TA^+) and a bromide counterion. At concentrations well below the critical micelle concentration (cmc = 0.92 mM), CTAB exists in the bulk water as fully dissociated unaggregated species. GFs on aqueous CTAB solutions are conformationally and translationally disordered at all concentrations and temperatures.

Alkanes are among the most common building blocks of all organic molecules, including lipids, surfactants, liquid crystals, and polymers. Despite their simple molecular structure, they exhibit a plethora of different ordered phases [6]. They also exhibit an intriguing surface freezing (SF) effect [7–10] in which a crystalline monolayer terminates the bulk melt's free surface for a range of temperature up to 3 °C *above* their bulk freezing temperature. SF in alkane melts is intimately related to the phenomena described in Langmuir-Gibbs films below.

Alkanes with $n > 6$ do not spread on the surface of pure water, but exist as isolated 3D lenses in equilibrium with a dilute 2D gas of alkane molecules [11]. However, sub-mM concentrations of CTAB induce a first-order wetting transition, wherein a mixed Langmuir-Gibbs film (LGF) of CTAB's alkyl tails and alkane molecules forms at the solution's surface. The long-range van der Waals interaction across the LGF (the disjoining pressure [12]) reduces its thickness below 1 nm. Thus, the LGF is in thermodynamical equilibrium with the lenses of the excess alkane molecules [13,14]. Novel phases and reversible order-disorder phase transitions are observed in this film upon cooling. For $11 \leq n \leq 17$, the LGF shows a first-order transition at temperatures up to 30 °C above the bulk melting point of the alkane. Ellipsometry [15] and sum-frequency vibrational spectroscopy [16] indicate that in the low-temperature phase the hydrocarbon chains are essentially all-*trans* chains and oriented normal to the water surface. We show here that this phase has a long-range hexagonal order. Moreover, for $n \geq 18$, the LGFs show a first-order transition to a bilayer structure and an ordered phase that has no parallel in any previously reported LF or GF. We characterize structurally this new phase, and show thermodynamically why this novel phase transition arises.

Figure 1 shows the coefficient of ellipticity $\bar{\rho}$ measured for CTAB-alkane LGFs. The sharp, hysteresis-free jumps observed indicate first-order phase transitions in the LGFs. The different size of the jumps for $n \leq 17$ and $n \geq 18$ implies films of different thickness in the lower temperature phase: a monolayer for $11 \leq n \leq 17$ [17], and a bilayer for $18 \leq n \leq 21$. The transition is also manifested in a change in the slope of the surface tension $\gamma(T)$ at the transition temperature T_s. Since the slope change equals the surface entropy loss upon ordering [7,10], the almost equal slopes observed for the monolayer (C_{16}) and the bilayer (C_{19}) phases imply that in both phases only a single layer orders at T_s. These inferences are supported by the x-ray measurements described below.

X-ray reflectivity (XR) and grazing incidence diffraction (GID) were employed to determine the structure of the monolayer and bilayer phases [10]. The XR curves $R(q_z)$ measured at a wavelength $\lambda \simeq 1.53$ Å, and normalized by

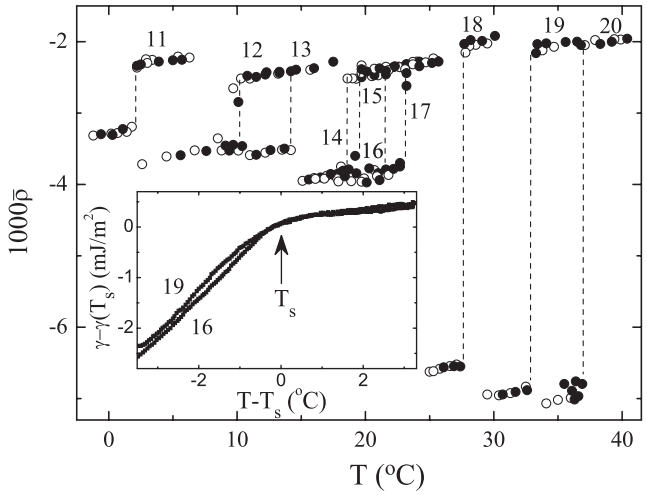

FIG. 1. Measured coefficient of ellipticity of LGFs for alkanes of length n. Open and closed symbols denote cooling and heating cycles, respectively. The jump indicates a phase transition with temperature, also manifested as a slope change in the surface tension $\gamma(T)$ (inset). Note the change in the size of the jump for $n \geq 18$.

the Fresnel XR of an ideal abrupt and smooth surface $R_F(q_z)$ are shown in Fig. 2(a). The surface-normal wave vector transfer $q_z = (4\pi/\lambda)\sin\alpha$ varies with α, the x-rays' grazing angle of incidence onto the surface. The observed modulations [18] arise from interference of x-rays reflected from the film's top and bottom interfaces. The surface-normal electron density profile $\rho_e(z)$ is obtained from $R(q_z)$ through a fit by a theoretical model [10]. The model fit [solid line, Fig. 2(a)] shows the alkane-free GF at the

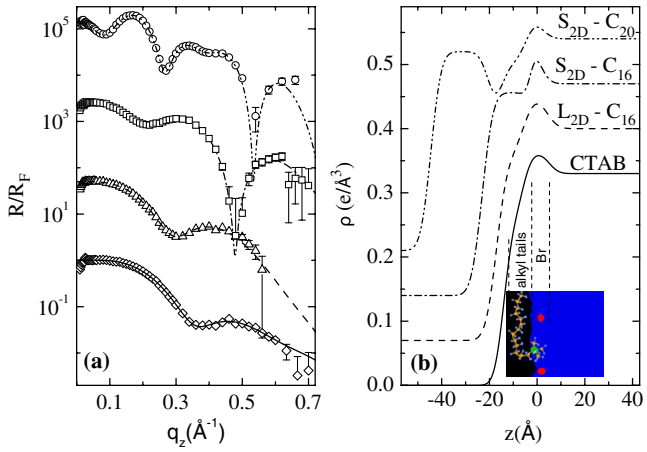

FIG. 2 (color online). (a) Measured Fresnel-normalized XR of bare CTAB GF (rhombi), liquid (triangles), and solid (squares) C_{16} + CTAB LGF, and solid C_{20} + CTAB LGF (circles). The model fits (lines) yield the same-line electron density profiles in (b). Cartoon: molecular interpretation (see text). $z = 0$ Å is defined as the Br^- ion distribution's peak position. Curves are shifted vertically from each other for clarity.

bare surface of the solution to consist of [see cartoon in Fig. 2(b)] a diffuse layer [19] of Br^- ions and a layer of C_{16} CTAB tails ($z < 0$), strongly smeared out by the capillary-waves-induced thermal roughness common to all liquid surfaces [10,20]. The (unsmeared) thickness of the hydrocarbon layer $d \approx 8$ Å is far smaller than the fully extended length $d_{C_{16}} = 21$ Å of a C_{16} chain, in agreement with earlier sum-frequency generation (SFG) [21] and neutron reflectivity measurements [22] showing the CTAB tails to be strongly disordered and tilted [15].

The LGF is formed by depositing hexadecane (C_{16}) dissolved in chloroform on the surface of the CTAB solution at $T = 26\,^\circ$C. The good minimum-to-maximum contrast obtained for this LGF [Fig. 2(a), triangles] demonstrates a uniform film thickness, and hence a good spreading of the alkane. The smaller q_z of the minimum implies that the LGF is thicker than the GF. Modeling (dashed line) yields an excellent fit with $d = 11.6$ Å, and a slightly higher ρ_e than for the bare GF. However, as $d \ll d_{C_{16}}$, the chains constituting the film, both CTAB and alkane, must be disordered and/or tilted [15]. The measured XR remains unchanged upon cooling down to $T = T_s = 22.5\,^\circ$C, where the reflectivity changes abruptly [squares, Fig. 2(a)]. The excellent model fit (dash-dotted line) yields the electron density profile $\rho_e(z)$ shown by the same line, Fig. 2(b). The surface layer is much thicker, with a value of $\rho_e = 0.31 \pm 0.02\ e/\text{Å}^3$, close to that of solid alkanes [23], and thickness $d = 20 \pm 1$ Å $\approx d_{C_{16}}$, strongly suggesting that at $T = T_s = 22.5\,^\circ$C a solid hydrocarbon layer forms. SFG measurements with selectively deuterated chains show that the hydrocarbon layer contains both alkanes and CTAB tails [15]. The sharp, single peak found at $q_\parallel = 1.516\ \text{Å}^{-1}$ in the GID measurements, which emerges at $T \leq T_s$, and the corresponding Bragg-rod (see Fig. 5 in [17]), unambiguously show the formation of a crystalline surface monolayer of a $\xi \gtrsim 1000$ Å crystalline coherence length [10]. Simple analysis reveals the GF monolayer to consist of extended, surface-normal chains, hexagonally packed in a quasi-2D crystal of an equivalent $4.785 \times 4.785\sqrt{3}$ Å^2 centered-rectangular unit cell, which coincides with that of the SF layer of a pure C_{16} melt [7,8,10]. The ellipsometry results (Fig. 1) are in excellent agreement with this model. The cartoon in Fig. 3(a) offers a molecular interpretation of the structure.

A longer alkane C_{20} yields $R(q_z)$ identical with that of C_{16} [triangles, Fig. 2(a)] for the liquid ($T > T_s = 37.8\,^\circ$C) LGF. However, in the surface-frozen phase $T \leq T_s$, the XRs are remarkably different [squares and circles, Fig. 2(a)]. The $\rho_e(z)$ obtained [dash-dot-dotted line, Fig. 2(b)] from the model fit [dash-dot-dotted line, Fig. 2(a)], and its molecular-level interpretation [cartoon in Fig. 3(b)], reveal the source of the difference. The C_{16} LGF remains, upon freezing, a mixed monolayer of extended CTAB and alkane chains. However, the C_{20} LGF

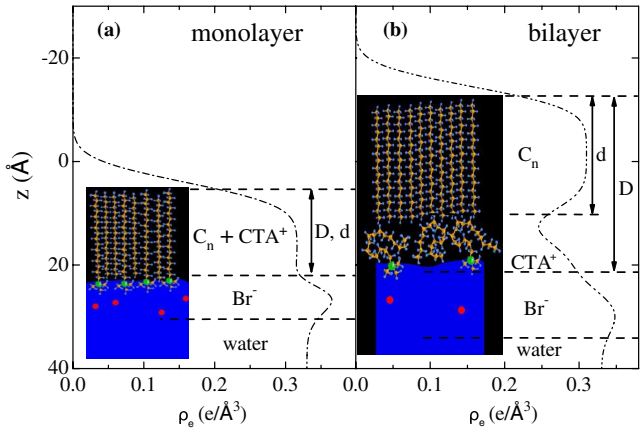

FIG. 3 (color online). XR-derived electron density profiles for C_{16} + CTAB monolayer (a) and C_{20} + CTAB bilayer (b) surface-frozen LGFs. Cartoons: molecular interpretation (see text).

forms a bilayer. The fit yields for the top layer $\rho_e = 0.31 \pm 0.01\ e/\text{Å}^3$ and $d = 26.4 \pm 1$ Å $= d_{C_{20}}$, implying a close-packed monolayer of extended C_{20} molecules. The bottom layer's $\rho_e = 0.28 \pm 0.02\ e/\text{Å}^3$ and $d = 13 \pm 1$ Å $\ll d_{C_{16}}$, close to those of the liquid phase, imply a layer of disordered chains. Indeed, the GID shows the surface-parallel order of the frozen C_{20} bilayer to be the same as that of the frozen C_{16} monolayer, discussed above. The Bragg rod of the GID peak corresponds to the length of a single C_{20} molecule, demonstrating that only the top layer is crystalline, with molecules aligned along the surface normal.

Although freezing of LGFs was first detected by ellipsometry [15], surface tension measurements $\gamma(T)$ using a Wilhelmy plate [7], provide important insight into the thermodynamics of this transition [7,10]. Typical $\gamma(T)$ curves are shown in Fig. 1(inset). The slope change at $T = T_s$ reflects the entropy loss upon LGF freezing: $\Delta S = d\gamma/dT|_{T<T_s} - d\gamma/dT|_{T>T_s}$ [7]. All values of ΔS obtained in this study coincide within ± 0.1 mJ/(m^2 K) with those measured (or linearly extrapolated into our n range) for SF in alkane melts [7,10], further supporting the conclusion that only a single monolayer freezes at T_s in both monolayer and bilayer phases.

XR measurements for C_n, $14 < n \leq 21$, show an n-independent thickness $d = 11.6 \pm 1$ Å [Fig. 4(a)] for the liquid phase, $T > T_s$, of all these n. This surprising result is supported by the near-n independence of the measured $\bar{\rho}$ at $T > T_s$ in Fig. 1. For the surface-frozen phase $T \leq T_s$, the XR-derived total hydrocarbon thickness D (defined in Fig. 3) reveals two distinct regimes: the monolayer regime $n \leq 17$, where $D = d$ and the crystalline monolayer comprises both CTAB tails and alkanes, and the bilayer regime $n \geq 18$, where $D > d$, the top crystalline layer comprise only alkanes, and the bottom layer is disordered. The perfect match in Fig. 4(a) between

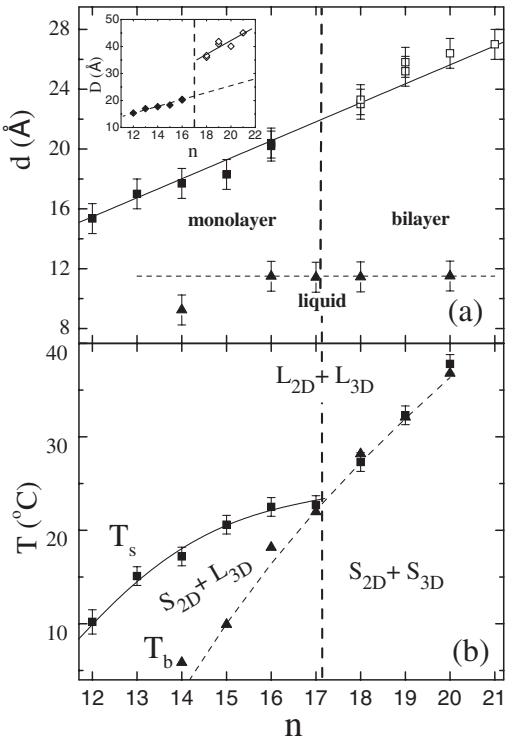

FIG. 4. (a) XR-derived thicknesses d and D (inset), defined in Fig. 3, in the frozen (squares) and the liquid (triangles) phases. Line—calculated extended length of alkane molecules. (b) The LGFs' (n, T) phase diagram. Phases are denoted as liquid (L) or solid (S) and film (2D) or droplet (3D). T_s and T_b (symbols) are the LGF's freezing, and the bulk's melting, temperatures, respectively. The vertical dashed line separates the monolayer and bilayer phases. The solid line is the theoretical T_s (see text).

the *crystalline* layer's thickness d in *both* regimes (squares) and the alkanes' calculated length (less the terminal H atom), $1.27(n-1) + 1.5$ Å [10,23] (solid line) proves that for $T \leq T_s$ the alkanes determine the crystalline layer's thickness for all n, their conformational degrees of freedom are frozen, and they are aligned roughly normal to the surface.

Figure 4(b) shows the (n, T) phase diagram. The measured $T_s(n)$ of the monolayer phase (squares, $n \leq 17$) can be explained by the simple thermodynamical theory of SF used for alkane mixtures [24]. The liquid LGF is treated as an ideal mixture, with a free energy including only the pure components' free energies and the mixing entropy. The solid phase of close-packed, extended chains is treated as a strictly regular mixture, with a free energy including also a CTAB-alkane interaction term. Equating the corresponding chemical potentials at T_s for each component [24] yields

$$T_s = [T_b(n)\Delta S_n - \omega x^2]/\{\Delta S_n + k_B \ln[(1-x)/(1-\phi)]\}$$
$$T_s = [T_b(16)\Delta S_C - \omega(1-x)^2]/\{\Delta S_C + k_B \ln[x/\phi]\}. \quad (1)$$

Here $T_b(n)$ and ΔS_n are the published [25] bulk melting

temperatures and entropies of C_n, ϕ (≈ 0.41 [15]) and x are the CTAB concentrations in the liquid and solid surface phases, and $\Delta S_C = \Delta S_{C_{16}}$ is the entropy loss per CTAB molecule upon freezing. The interchange energy $\omega = a + b(\Delta n/\bar{n})^2$ comprises a chain length mismatch (Δn) term [24], and a constant ion(CTA^+)-alkane interaction term a. Thus, within this model, the CTAB differs thermodynamically from a C_{16} molecules only by the headgroup interaction energy a. Replacing CTAB by the C_{18}-tailed STAB shifts the bilayer formation from $n \geq 18$ to $n \geq 20$, further supporting the dependence of ω on Δn. Solving Eqs. (1) for T_s and x by fitting to the measured T_s values yields $a = -1.7k_BT$, $b = 26k_BT$, and the solid line in Fig. 4(b). The agreement with the measured T_s is remarkably good. x varies from 0.66 ($n = 12$) to 0.4 ($n = 17$), in agreement with a limiting surface area of ~ 32 Å^2 per cation [26]. The negative a reveals an effective CTA^+-alkane *attraction*, in contrast with alkane mixtures [24], where $\omega > 0$, and unlike molecules repel each other in all mixtures.

The formation of the bilayer can be explained by noting that the free surface of the disordered, liquidlike mixed monolayer at $T < T_s$ is akin to the free surface of a molten bulk alkane. Thus, the wetting of this layer's top surface by a solid monolayer of pure alkanes closely resembles the wetting of the alkane melt's surface by a solid monolayer upon ''conventional'' SF [27]. This plausibly explains the formation of the bilayer phase for $n \geq 18$. For $n \leq 17$, this wetting transition is preempted by the mixed monolayer's freezing transition discussed above. The explanation above may account also for a related effect wherein a frozen monolayer forms at the interface between a *bulk* alkane phase and bulk CTAB solution phase for alkanes of $n \leq 15$. However, for larger n, the absence of a free surface should suppress the bilayer phase, and it is indeed not observed [28].

The novel wetting properties and phase diagram of LGFs presented here may be further tuned by varying the surfactant's molecular architecture and bulk concentration, thus providing deeper insight into the intriguing phase behavior and structure of Langmuir-Gibbs films.

Support by the U.S.-Israel Binational Science Foundation, Jerusalem, is gratefully acknowledged. BNL is supported by U.S. DOE Contract No. DE-AC02-98CH10886.

*deutsch@mail.biu.ac.il

[1] A. Pockels, Nature (London) **43**, 437 (1891).
[2] *Molecular Electronics*, edited by J. Jortner and M. Ratner (Blackwell, Oxford, 1997); A. S. Martin, J. R. Sambles, and G. J. Ashwell, Phys. Rev. Lett. **70**, 218 (1993); S. N. Shtykov and T. Yu. Rusanova, Dokl. Phys. Chem. **388**, 60 (2003).
[3] V. M. Kaganer, H. Möhwald, and P. Dutta, Rev. Mod. Phys. **71**, 779 (1999).
[4] B. Widom, Physica (Amsterdam) **95A**, 1 (1979).
[5] J. Penfold *et al.*, Langmuir **20**, 2265 (2004).
[6] E. B. Sirota and A. B. Herhold, Science **283**, 529 (1999).
[7] X. Z. Wu *et al.*, Science **261**, 1018 (1993).
[8] J. C. Earnshaw and C. J. Hughes, Phys. Rev. A **46**, R4494 (1992); X. Z. Wu *et al.*, Phys. Rev. Lett. **70**, 958 (1993).
[9] C. Merkl, T. Pfohl, and H. Riegler, Phys. Rev. Lett. **79**, 4625 (1997); N. Maeda and V. V. Yaminsky, *ibid.* **84**, 698 (2000); Y. Shinohara *et al.*, *ibid.* **94**, 097801 (2005); S. Prasad and A. Dhinojwala, *ibid.* **95**, 117801 (2005).
[10] B. M. Ocko *et al.*, Phys. Rev. E **55**, 3164 (1997).
[11] D. Bonn and D. Ross, Rep. Prog. Phys. **64**, 1085 (2001).
[12] J. N. Israelachvili, *Intramolecular and Surface Forces* (Academic, San Diego, 1992).
[13] J. R. Lu *et al.*, J. Chem. Phys. **99**, 4113 (1995); R. Aveyard *et al.*, J. Chem. Soc., Faraday Trans. **86**, 3623 (1990); H. Matsubara *et al.*, Langmuir **22**, 982 (2006).
[14] K. M. Wilkinson *et al.*, Chem. Phys. Chem. **6**, 547 (2005).
[15] K. M. Wilkinson, Q. Lei, and C. D. Bain, Soft Matter **2**, 66 (2006).
[16] C. McKenna, M. M. Knock, and C. D. Bain, Langmuir **16**, 5853 (2000).
[17] E. Sloutskin *et al.*, Thin Solid Films **515**, 5664 (2007) discusses the monolayer's properties.
[18] M. Born and E. Wolf, *Principles of Optics* (Pergamon, Oxford, 1980).
[19] W. Bu, D. Vaknin, and A. Travesset, Phys. Rev. E **72**, 060501(R) (2005).
[20] B. M. Ocko *et al.*, Phys. Rev. Lett. **72**, 242 (1994).
[21] G. R. Bell, S. Manning-Benson, and C. D. Bain, J. Phys. Chem. B **102**, 218 (1998).
[22] J. R. Lu *et al.*, J. Phys. Chem. **99**, 8233 (1995); **97**, 6024 (1993).
[23] D. M. Small, *The Physical Chemistry of Lipids* (Plenum, New York, 1986).
[24] E. Sloutskin *et al.*, Phys. Rev. Lett. **89**, 065501 (2002); E. Sloutskin *et al.*, Phys. Rev. E **68**, 031605 (2003) [see derivation in Sec. III(b)]; E. Sloutskin *et al.*, Eur. Phys. J. E **13**, 109 (2004).
[25] As LGFs exhibit only rotator phases, $T_b(n)$ and ΔS_n values for even n (freezing into a crystalline phase) were interpolated from odd ones (freezing into a rotator phase) [23] to avoid odd-even effects.
[26] B. Jańczuk *et al.*, Tenside Surf. Det. **35**, 213 (1998).
[27] E. B. Sirota *et al.*, Phys. Rev. Lett. **79**, 531 (1997).
[28] Q. Lei and C. D. Bain, Phys. Rev. Lett. **92**, 176103 (2004); E. Sloutskin *et al.*, Faraday Discuss. **129**, 339 (2005).